

Study of Interplanetary Magnetic Field with Atomic Alignment

Jinyi Shangguan^{1*} and Huirong Yan^{2†}

¹*Department of Astronomy, School of Physics, Peking University, Beijing, 100871, China*

²*KIAA, Peking University, Beijing, 100871, China*

8 February 2022

ABSTRACT

We demonstrate a new way of studying interplanetary magnetic field – atomic alignment. Instead of sending thousands of space probes, atomic alignment allows magnetic mapping with any ground telescope facilities equipped with spectro-polarimeter. The polarization of spectral lines that are pumped by the anisotropic radiation from the sun is influenced by the magnetic alignment, which happens for weak magnetic field ($< 1\text{ G}$). As a result, the line polarization becomes an excellent tracer of the embedded magnetic field. The method is illustrated by the specific cases of Io and comet Halley that we consider. Magnetometer data from the Galileo mission Io flyby (2002) were used in order to construct the topology of the magnetic field around Jupiter. So as to the data from the vega mission comet Halley flyby(1986). A uniform density distribution of Na was considered and polarization at each point was then constructed. Both spatial and temporal variations of turbulent magnetic field can be traced with this technique as well. For remote regions like the the boundary with interstellar medium, atomic alignment provides a unique diagnostics of magnetic field, which is crucial for understanding the physical processes like the IBEX ribbons discovered recently.

Key words: interplanetary medium, magnetic fields, atomic processes, scattering, techniques: polarimetric

1 INTRODUCTION

Magnetic fields are ubiquitous and play extremely important roles in many astrophysical circumstances, e.g., the interstellar medium, intergalactic medium, and quasars. In the mean time, there are only a few techniques for magnetic field studies that are available. Each technique is sensitive to magnetic fields in particular environments and has its own limitations. Therefore, even the directions of a magnetic field obtained for the same region of sky with different techniques differ substantially. The simultaneous use of different techniques provides a possibility of magnetic field tomography.(see Yan, & Lazarian 2006 for details)

Interplanetary magnetic field is turbulent with complicated spacial and temporal variations. However, it is always important or unavoidable when considering the interplanetary processes. For instance, we have to deal with the coherence of the plasma and the magnetic field when studying the interplanetary medium. The interplanetary current sheet is created by the magnetic field’s rotation and reconnection. The comic rays can be obviously influenced by the interplanetary magnetic field.

The recently launched NASA’s satellite Interstellar Boundary Explorer (IBEX) (McComas et al. 2009) discovered a bright narrow “ribbon” of energetic neutral atoms (ENA) emission nearly across the entire celestial sphere, which is unpredicted by any prior models or theories. It has been shown that this ribbon is largely stable, with small time variations, which implies a sustained local magnetic structure interacting with the original solar magnetic field (Funsten et al. year and Schwadron et al. 2009). Galactic magnetic field immediately outside the heliopause’s special orientation might result in the “ribbon” structure.(see Heerikhuisen et al. 2010). The heliosphere is asymmetric as the two Voyager spacecraft detected when crossing the termination shock (see Stone et al. 2005), indicating the significance of magnetic field in the dynamic process of the outer heliosphere. But as far as we know, there is no direct measurement of the magnitude and orientation of the magnetic field in those region.

Atomic alignment is a new promising way of studying magnetic fields in radiation-dominated environments. In fact, this diagnostic is far more sensitive than those based on the Zeeman effect. The basic idea of atomic alignment is simple: consider atoms irradiated by a nearby

* shangguan@pku.edu.cn

† hryan@pku.edu.cn

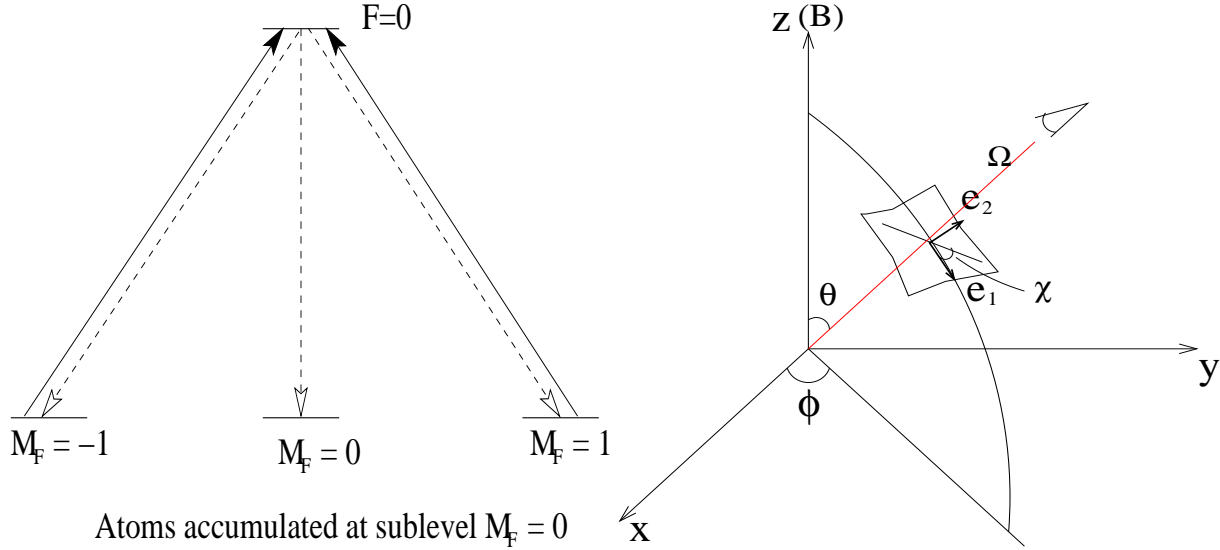


Figure 1. *Left:* a toy model to illustrate how atoms are aligned by anisotropic light. Atoms accumulate in the ground sublevel $M = 0$ as radiation removes atoms from the ground states $M = 1$ and $M = -1$; *Right:* radiation geometry and the polarization vectors in a given coordinate system. Ω is the direction of radiation, χ is the positional angle of a linear polarization.

star and embedded in a magnetic field. Anisotropic radiation pumps the atoms differentially from different magnetic sublevels, resulting in over- or underpopulations of the atomic states of various magnetic quantum numbers, M . Then the absorbed and scattered light will get polarized by the aligned atoms, relying on the magnetic field, especially the direction, around them. So it's an effective way to obtain the 3D orientation of magnetic field and a cost efficient method, just by detecting the polarization of light from the object rather than sending a satellite.

In this paper, we first discuss a synthetic observation of Jupiter's magnetic field that has been detected by Galileo spacecraft. The third largest of Jupiter's moons, Io, is chosen as the tracer of our synthetic observation, since it has been shown that there is abundant sodium in the wake of Io. Secondly we give the result of synthetic observation of the Comet Halley. The alignment of sodium was calculated particularly in Yan, & Lazarian (2007). Here, we use the D2 emission line of sodium (*high resolution*). We also consider the situation when the spectrometer cannot resolve the D1 and D2 lines (*low resolution*). Since D1 line is unpolarized, the polarization degree in the case of low spectral resolution is reduced.

Galileo spacecraft was sent to Jupiter for an 8-year mission in Jovian system. It detected Io and other moons of Jupiter, sending abundant information about the Jovian system. One of them is the magnetic field. We downloaded the data from NASA PDS-PPI (see Kivelson et al. 1997).

Vega spacecrafts (vega1 and vega2) were sent to Venus and to Comet Halley was implemented by the USSR with international participation. The main spacecraft encounter with Comet Halley was in March 6 and 9, 1986. Data were obtained during both the encounter and cruise phases of the mission.¹

Undoubtedly, compared to the vast interplanetary space that magnetic fields prevail, the information we can get from space crafts is far less adequate. With these studies, we try to demonstrate atomic alignment as an easy, but powerful magnetic diagnostics. It enables a tomography of interplanetary magnetic field without sending thousands of space probes.

In what follows, we first discuss the basic idea of atomic alignment, giving some important formula that is necessary for our synthetic observation in §2. Then talk a little about the frame rotation in §3, which is simple but sometimes confusing. We present the observation result of the magnetic field traced by Io in §4 and discuss the advantage of atomic alignment to detect the interplanetary magnetic field. The synthetic observation of Comet Halley is discussed in §5. The discussion and the summary are provided in, respectively, §6 and §7.

2 BRIEF INTRODUCTION OF ATOMIC ALIGNMENT

The basic idea of the atomic alignment² is quite simple. The alignment is caused by the anisotropic deposition of angular momentum from photons. In typical astrophysical situations the radiation flux is anisotropic. As the photon spin is along the direction of its propagation, we expect that atoms scattering the radiation from a light beam to be aligned. Such an alignment happens in terms of the projections of angular

¹ see ftp://nssdcftp.gsfc.nasa.gov/spacecraft_data/vega/mag/

² Since the alignment of atom and ion are generally the same, atom represents both of them in this paper

momentum to the direction of the incoming light. For atoms to be aligned, their ground state should have nonzero angular momentum. Therefore, fine (or hyperfine) structure is necessary to enable various projection of atomic angular momentum to exist in their ground state.

Let us discuss a toy model, that provides an intuitive insight in the physics of atomic alignment. Consider an atom with its ground state corresponding to the total angular momentum $I=1$ and the upper state corresponding to the angular momentum $I=0$ (see Varshalovich et al. 1968). If the projection of the angular momentum to the direction of the incident resonance photon beam is M , the lower state M can have values $-1, 0$, and 1 , while for the upper state $M=0$ (see Fig.1 *left*). The unpolarized beam contains an equal number of left and right circularly polarized photons whose projections on the beam direction are 1 and -1 .

Thus, absorption of the photons will induce transitions from the $M=-1$ and 1 sublevels. However, the decay from the upper state populates all three sublevels of the ground state. As a result, the atoms accumulate in the $M=0$ ground sublevel from which no excitations are possible. Accordingly, the optical properties of the media (e.g. absorption and scattering) would change.

The above toy model can also exemplify the role of collisions and magnetic field. Without collisions one may expect that all atoms reside eventually at the sublevel of $M=0$. Collisions, however, redistribute atoms to different sublevels. Nevertheless, as disalignment of the ground state requires spin flips, it is less efficient than one might naively imagine (Hawkins 1955). The reduced sensitivity of aligned atoms to disorienting collisions makes the effect important for various astrophysical environments.

All in all, in order to be aligned, first, atoms should have enough degrees of freedom; namely, the quantum angular momentum number must be 1 . Second, the incident flux must be anisotropic. Moreover, the collisional rate should not be too high. While the latter requires special laboratory conditions, it is applicable to many astrophysical environments such as the interplanetary medium, the outer layers of stellar atmospheres, the ISM, and the intergalactic medium.

For the optically thin case, the linear polarization degree and the positional angle are

$$p = \sqrt{Q^2 + U^2}/I = \sqrt{\epsilon_2^2 + \epsilon_1^2/\epsilon_0}, \quad \chi = \frac{1}{2} \tan^{-1}(U/Q) = \frac{1}{2} \tan^{-1}(\epsilon_2/\epsilon_1) \quad (1)$$

(see Fig.1 *right*), where ϵ_i ($i = 1, 2, 3$) are emission coefficients. As to the alignment of Sodium, things get somehow complicated. Since Sodium has nuclear spin $I = 3/2$, we should consider the total momentum $F = J + I$, thus hyperfine structure is taken into consideration. We can obtain the emission coefficients (see Yan, & Lazarian (2007)) for detail calculation) of each hyperfine structure as below. For D2 line, $F_I = 1$,

$$\begin{aligned} \epsilon_0 &= \frac{3\sqrt{3}\lambda^2}{8\pi} A_{I_s} n p_0^0 \xi(v-v_0) \left\{ 62830 - 10084 \cos 2\theta_r - 412 \cos 4\theta_r + (30.3 \cos 4\theta_r + 2236.6 \cos 2\theta_r + 776) \cos 2\theta + \cos 2\theta_r [(395 - 513.4 \cos 2\theta_r + 107.4 \cos 4\theta_r) \sin^2 \theta] + \cos \phi_r [104.3 \right. \\ &+ 1.95 \cos 2\theta_r - 212.19 \cos 4\theta_r + 8.5(\cos 2\theta_r - 1.4 \cos 4\theta_r + 48.5) \sin 2\theta \sin 2\theta_r] \} \\ \epsilon_1 &= -\frac{3\sqrt{3}\lambda^2}{8\pi} A_{I_s} n p_0^0 \xi(v-v_0) \left\{ (1552.7 + 4473.3 \cos 2\theta_r + 60.6 \cos 4\theta_r) \sin^2 \theta + \cos 2\theta_r [592.5 + \cos 2\theta (197.5 + 53.7 \cos 4\theta_r - 256.7 \cos 2\theta_r) - 770.1 \cos 2\theta_r + 161.1 \cos 4\theta_r] \right. \\ &+ \cos \phi_r (17.0 \cos 2\theta_r - 23.8 \cos 4\theta_r) \sin 2\theta \sin 2\theta_r \} \\ \epsilon_{27} &= -\frac{3\sqrt{3}\lambda^2}{8\pi} A_{I_s} n p_0^0 \xi(v-v_0) [\cos \theta (790 - 1026.9 \cos 2\theta_r + 214.8 \cos 4\theta_r) \sin 2\theta_r + (34.0 \cos 2\theta_r - 47.6 \cos 4\theta_r + 1649.9) \sin \phi_r \sin \theta \sin 2\theta_r] \end{aligned} \quad (2)$$

$F_I = 2$,

$$\begin{aligned} \epsilon_0 &= \frac{3\sqrt{3}\lambda^2}{8\pi} A_{I_s} n p_0^0 \xi(v-v_0) \left\{ 136670 - 28893 \cos 2\theta_r + 899 \cos 4\theta_r + \cos^2 \theta (20729 \cos 2\theta_r - 1118 \cos 4\theta_r + 6057) + \cos 2\theta_r (5649.4 - 6278.5 \cos 2\theta_r \right. \\ &+ 656.2 \cos 4\theta_r) \sin^2 \theta + \cos \phi_r [2522.6 - 147.8 \cos 2\theta_r - 2521.1 \cos 4\theta_r + (5090 - 591 \cos 2\theta_r + 6 \cos 4\theta_r) \sin 2\theta \sin 2\theta_r] \} \\ \epsilon_1 &= -\frac{3\sqrt{3}\lambda^2}{8\pi} A_{I_s} n p_0^0 \xi(v-v_0) \left\{ (20729 \cos 2\theta_r - 1117.7 \cos 4\theta_r + 6057.1) \sin^2 \theta + \cos 2\theta_r [(-6278.5 \cos 2\theta_r + 656.2 \cos 4\theta_r + 5649.4) \cos^2 \theta - 6479.6 \cos 2\theta_r + 656.2 \cos 4\theta_r + 5649.4] \right. \\ &+ \cos \phi_r (10097 - 1183.0 \cos 2\theta_r + 12.4 \cos 4\theta_r) \sin 2\theta \sin 2\theta_r + 6057.1 \} \\ \epsilon_2 &= -\frac{3\sqrt{3}\lambda^2}{8\pi} A_{I_s} n p_0^0 \xi(v-v_0) \left\{ \cos \theta (20189 - 4818 \cos 2\theta_r + 215 \cos 4\theta_r) \sin^2 \theta_r \sin 2\theta_r + (20193 - 2366 \cos 2\theta_r + 25 \cos 4\theta_r) \sin \phi_r \sin \theta \sin 2\theta_r \right\} \end{aligned} \quad (3)$$

For D1 line, $F_I = 1$,

$$\begin{aligned} \epsilon_0 &= \frac{3\sqrt{3}\lambda^2}{8\pi} A_{I_s} n p_0^0 \xi(v-v_0) \left\{ 36142 - 6350 \cos 2\theta_r - 285 \cos 4\theta_r - \cos 2\theta (40 + 76 \cos 4\theta_r + 26 \cos 2\theta_r) - \cos 2\theta_r [(588 - 702 \cos 2\theta_r + 126 \cos 4\theta_r) \sin^2 \theta] - \cos \phi_r [268 - 1.19 \cos 2\theta_r - 267 \cos 4\theta_r \right. \\ &+ (537.0 - 5.1 \cos 2\theta_r + 2.7 \cos 4\theta_r) \sin 2\theta \sin 2\theta_r] \} \\ \epsilon_1 &= -\frac{3\sqrt{3}\lambda^2}{8\pi} A_{I_s} n p_0^0 \xi(v-v_0) \left\{ (130.89 \cos 2\theta_r - 153.45 \cos 4\theta_r - 2050.2) \sin^2 \theta + \cos 2\theta_r [\cos 2\theta (-293.92 - 62.56 \cos 4\theta_r + 251.03 \cos 2\theta_r) + 1053.08 \cos 2\theta_r - 187.674 \cos 4\theta_r \right. \\ &- 881.772] - \cos \phi_r [1073.92 - 10.216 \cos 2\theta_r + 5.472 \cos 4\theta_r] \sin 2\theta \sin 2\theta_r + 1969.6 \} \\ \epsilon_2 &= -\frac{3\sqrt{3}\lambda^2}{8\pi} A_{I_s} n p_0^0 \xi(v-v_0) [1404.1 \cos \theta (\cos 2\theta_r - 0.1782 \cos 4\theta_r - 0.8373) \sin 2\theta_r + (20.4 \cos 2\theta_r - 10.9 \cos 4\theta_r - 2147.8) \sin \phi_r \sin \theta \sin 2\theta_r] \end{aligned} \quad (4)$$

$F_I = 2$,

$$\begin{aligned} \epsilon_0 &= \frac{3\sqrt{3}\lambda^2}{8\pi} A_{I_s} n p_0^0 \xi(v-v_0) \left\{ 64488 - 10148 \cos 2\theta_r + 337 \cos 4\theta_r - \cos 2\theta (-66.73 \cos 4\theta_r + 65.45 \cos 2\theta_r - 40.301) - \cos 2\theta_r [(-587.8 + 702 \cos 2\theta_r - 125.2 \cos 4\theta_r) \sin^2 \theta] \right. \\ &+ \cos \phi_r [268 - 1.19 \cos 2\theta_r - 267.1 \cos 4\theta_r + \sin 2\theta \sin 2\theta_r (536.96 - 5.11 \cos 2\theta_r + 2.74 \cos 4\theta_r)] \} \\ \epsilon_1 &= -\epsilon_2 (F_I = 1) \\ \epsilon_2 &= -\epsilon_2 (F_I = 1) \end{aligned} \quad (5)$$

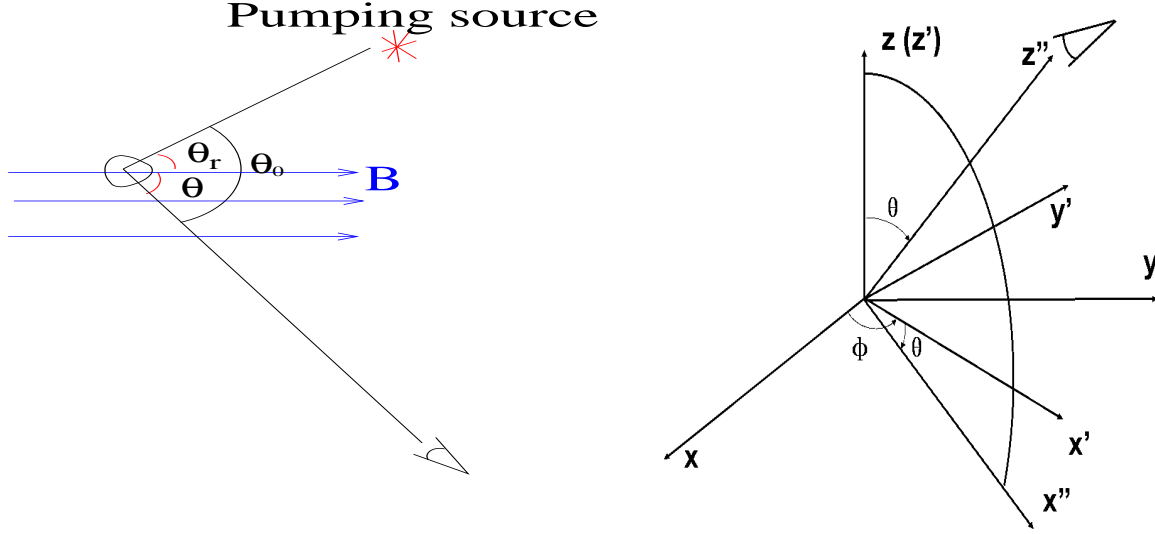


Figure 2. *Left:* typical astrophysical environment where atomic alignment can happen. A pumping source deposits angular momentum to atoms in the direction of radiation and causes differential occupations on their ground states. In a magnetized medium where the Larmor precession rate ν_L is larger than the photon arrival rate τ_R^{-1} , however, atoms are realigned with respect to magnetic field. Atomic alignment is then determined by θ_r , the angle between the magnetic field and the pumping source. The polarization of scattered line also depends on the direction of line of sight, θ and θ_0 (or ϕ_r , defined afterward). *Right:* The xyz-frame is JSO (or CSE) frame in which the data were detected. We firstly need to transmit the magnetic data and the space coordinates into observational frame. This can be done by two successive rotations specified by Euler angles (θ, ϕ) . The first rotation is from xyz coordinate system to $x'y'z'$ coordinate system by an angle ϕ about the z-axis, the second is from $x'y'z'$ coordinate system to $x''y''z''$ coordinate system by an angle θ about the y' -axis.

3 FRAME ROTATION

Since the theoretical calculation of alignment is generally in different frame from the observational data recorded in, some frame rotations are necessary. (see Fig.1 *right*, Fig.2 *right* and Fig.3 *right*) We get Jupiter's magnetic data from NASA PDS-PPI in two separate frames, JSO (Jupiter Solar Orbital)³ and SYS3 (system III) both of whose instruction can be found in the corresponding website with the data.⁴ The significant difference between the two frames is that SYS3 frame is rotating together with Jupiter, the period of which is about 9 and a half hours, while the JSO frame is rest in Jupiter-Sun system. So the relative position of the sun, the Jupiter and the earth can approximate to be quiescent, since the revolution of both the Jupiter and the earth is quite long compared with the time used for collecting the magnetic field data. The facility of choosing those two frames is that data in SYS3 can show us the map of Jupiter's magnetic field, even though it can merely give a qualitative impression. And the data in JSO frame can gives the picture of polarization corresponding to the magnetic field in observational frame on the earth, which we mainly employ. For the case of Comet Halley, the coordinate frame is CSE (CometoCenter Solar Ecliptic)⁵, almost the same as JSO except that the center object is the comet.

Some initial conditions are necessary, which are the position angle of the sun (the pumping source) and the position angle of the earth in JSO (or CSE) frame. Since the x-axis is defined along the radial from Jupiter(or Comet Halley) to the sun, the position angle of the sun is simply $(0^\circ, 0^\circ)$. We choose the earth is to be at $(83^\circ, 5^\circ)$ in the case of Jupiter and $(60^\circ, 5^\circ)$ in the case of Comet Halley. Since this is just a synthetic observation, the coordinates are not accurate.

In terms of the synthetic observation, we need to obtain θ_r and ϕ_r which are crucial for calculating polarization. Firstly we need to transform all magnetic field data (from JSO frame) into the observational frame (see Fig.2 *right*), since the calculation of emission coefficients are based on the frame. (see Fig.3 *right*) And it's worthy to mention that all the figures below that's in x-y plane corresponds to the observational frame here we received. Secondly, in order to obtain θ_r and ϕ_r , we transform the observational frame to the theoretical frame (Fig.1 *right*) which are generally various in different position subjected to the direction of magnetic field. In general, those two rotations are the same and can be done by two Euler rotations, as illustrated in Fig.2 *right* and Fig.3 *right*. Mathematically, the two rotations from observational frame to the theoretical frame can be fulfilled by multiplying rotation matrixes,

$$\begin{bmatrix} \cos \theta & 0 & -\sin \theta \\ 0 & 1 & 0 \\ \sin \theta & 0 & \cos \theta \end{bmatrix} \begin{bmatrix} \cos \phi_B & \sin \phi_B & 0 \\ -\sin \phi_B & \cos \phi_B & 0 \\ 0 & 0 & 1 \end{bmatrix} = \begin{bmatrix} \cos \theta \cos \phi_B & \cos \theta \sin \phi_B & -\sin \theta \\ -\sin \phi_B & \cos \phi_B & 0 \\ \sin \theta \cos \phi_B & \sin \theta \sin \phi_B & \cos \theta \end{bmatrix} \quad (6)$$

³ In JSO coordinates, X points from Jupiter to the Sun. Z is parallel to the Jupiter orbital plane upward normal. Y completes the right handed set.

⁴ see http://pds-ppi.igpp.ucla.edu/inventory.jsp?volume=GOMW_5005&folder=DATA/MAG/SURVEY/REALTIME&file=ORB32_JS0_JSM

⁵ In CSE coordinates, the origin is at comet position, x-axis is from comet to the Sun, z-axis is to ecliptic northpole, (x,y)-plane is parallel to the ecliptic plane.

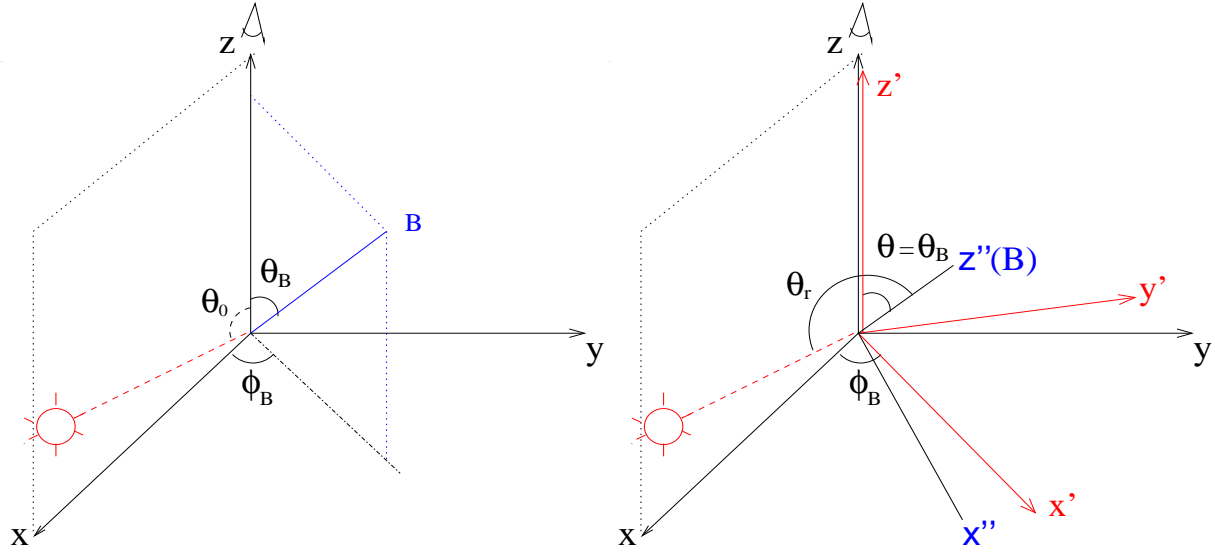


Figure 3. *Left:* geometry of the observational frame. In this frame, the line of sight is z axis. The incident light is in (θ_0, ϕ_0) direction. Magnetic field is in (θ_B, ϕ_B) direction; *Right:* transformation to the "theoretical frame" where magnetic field defines z'' axis. The process of rotation is the same as Fig.2 right. Thus, The first rotation is from xyz coordinate system to $x'y'z'$ coordinate system by an angle ϕ_B about the z -axis, the second is from $x'y'z'$ coordinate system to $x''y''z''$ coordinate system by an angle θ_B about the y' -axis. Atomic alignment and transitions are treated in the "theoretical" frame where the line of sight is in (θ, π) direction and the incident radiation is in (θ_r, ϕ_r) direction.(see Fig.1 right and Fig.2 left)

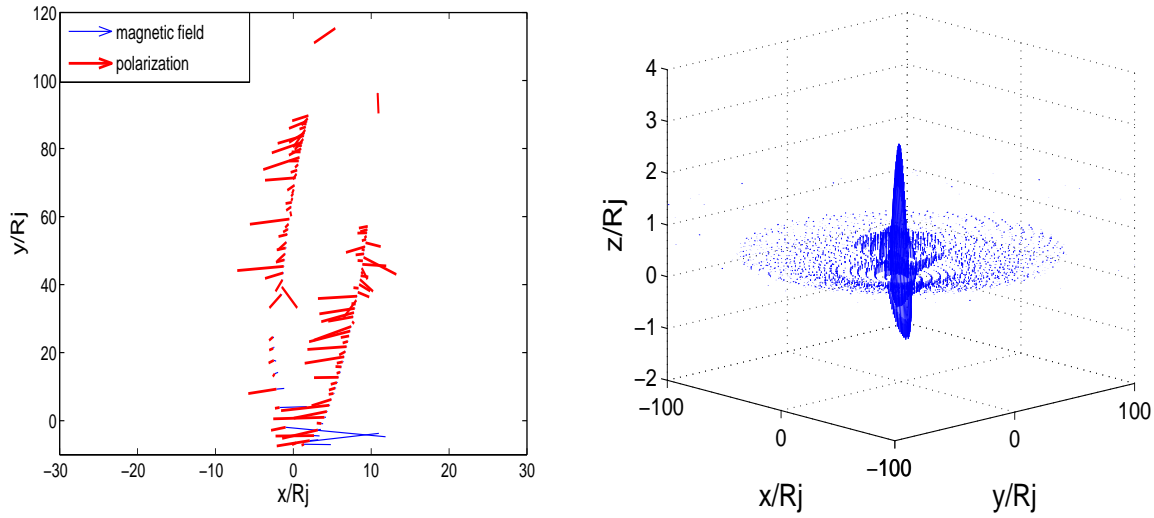


Figure 4. *Left:* the synthetic observation result in celestial coordinate, where red thick line represents the polarization direction and blue thin line represents the direction of magnetic field. The unit of the coordinates is $R_j = 71492$ km. *Right:* the magnetic field detected by Galileo, represented by the same data with the left panel but in SYS3 frame. It can give us the qualitative impression of the Jupiter's magnetic field.

The rotations from JSO (or CSE) frame to observational frame are all the same. You can just change ϕ_B to ϕ to obtain the transform matrix according to Fig.2 right. We obtain the position angle of pumping source in theoretical frame,

$$\theta_r = \arccos(\sin \theta \cos \phi_B \sin \theta_0 \cos \phi_0 + \sin \theta \sin \phi_B \sin \theta_0 \sin \phi_0 + \cos \theta \cos \theta) \quad (7)$$

$$\phi_r = \arcsin((- \sin \phi_B \sin \theta_0 \cos \phi_0 + \cos \phi_B \sin \theta_0 \sin \phi_0) / \sin \theta_r) \quad (8)$$

where θ equals θ_B and (θ_0, ϕ_0) is the position angle of the pumping source in observational frame. (see Fig.3)

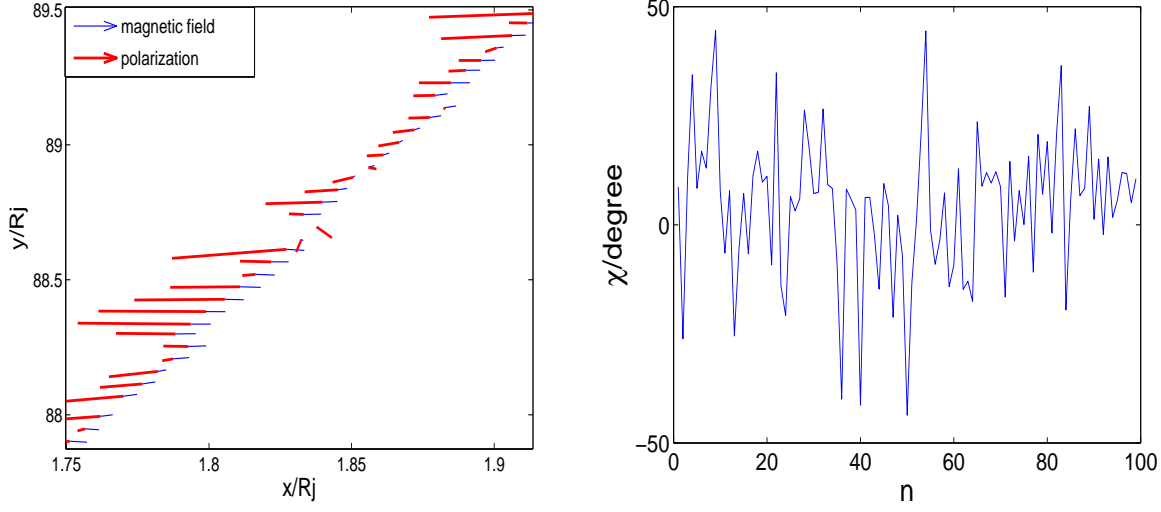


Figure 5. *Left:* a local part of the Fig.4 left which distinguish the blue thin lines. *Right:* the acute angle between the polarization vector and the projection line of the magnetic field vector to the celestial coordinate plane. To ensure the clarity of the figures, we use lines instead of arrows to represent the vectors.

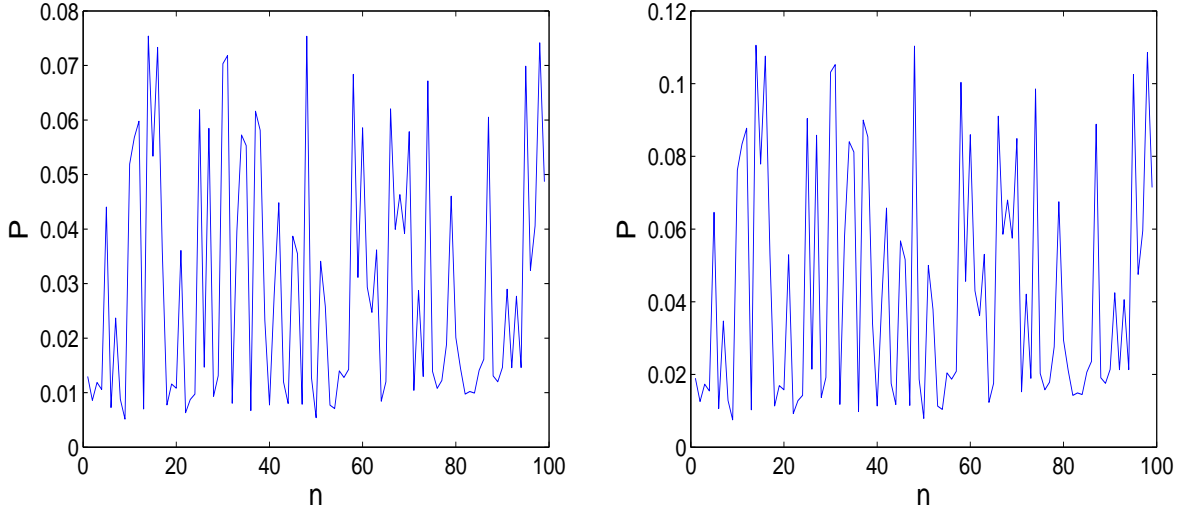


Figure 6. *Left:* the polarization degree of low resolution. *Right:* the polarization degree of high resolution. n of the x-axis is the sequence number of the data corresponding to Fig.4 left. The two panels correspond to Fig.4 Left.

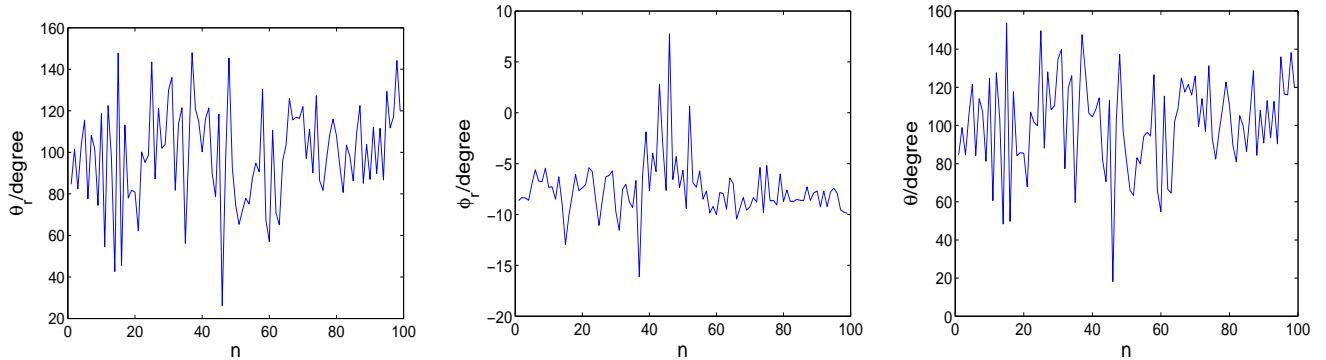


Figure 7. *Left:* θ_r , the angle between incident radiation and magnetic field see Fig.2 left and Fig.3 right. *Middle:* ϕ_r , the azimuth of the incident radiation corresponding to θ_r in the theoretical frame. *Right:* θ , the angle between the observational direction and the magnetic field.

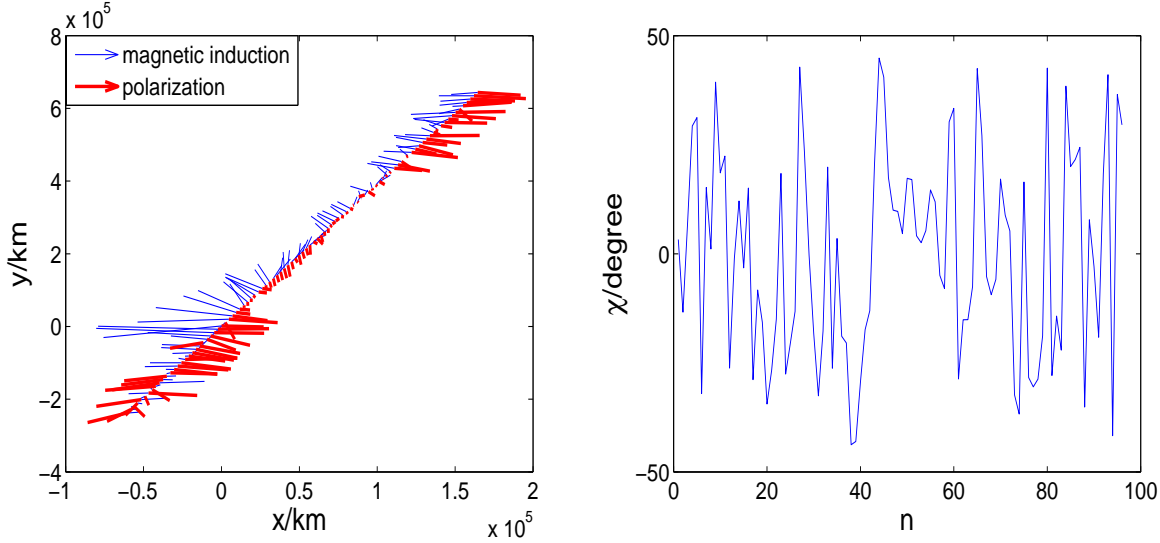


Figure 8. *Left:* the Magnetic field and polarization along the trajectory of vega1 near the comet Halley. The blue thin lines represent magnetic field and the red thick lines represent the polarization vectors. The x-y plane is the plane of celestial coordinates. *Right:* the acute angle between the polarization vector and the projection line of the magnetic field vector to the celestial coordinate plane. n of the x-axis is the sequence number of the data, corresponding to the left panel.

4 SYNTHETIC OBSERVATION

Since spacecrafts can only get the local information of magnetic field on its orbit, our synthetic observation shall follow the trajectory of spacecrafts. Magnetic field increases sharply when it goes near Jupiter, as shown in Fig.4 *right*. Correspondingly, the blue thin lines are distinct only at the bottom of Fig.4 *left* which locates near Jupiter, although magnetic field exist everywhere. In order to reveal the relationship of the magnetic field and the polarization, we chose and magnified a local part of the Fig.4 *left* as Fig.5 *left*. χ , the acute angle between the polarization vectors (red thick lines) and the projection of the magnetic field in the celestial coordinate plane (blue thin lines, Fig.5 *right*), varies in the range of ± 50 degree (see Yan, & Lazarian (2007)). For the *low resolution*, the average polarization degree is around 3 %, while it can reach as high as 7.5 % and as low as 0.5 % (see Fig.6 *left*). Fig.6 *right* shows us the polarization degree at *high resolution*, whose polarization degrees are generally higher than *low resolution*'s, since the light of D1 line is unpolarized. The mean polarization degree is 4.3 %, while it can reach 11.1 % to the most and 0.8 % to the least. It's easy to find that the shapes of the polarization degree figure at *high* and *low* resolution is the same, the difference is the range. The similarity of Fig.7 *left* with *right* is rational since there isn't much difference in the position angles of the sun and the earth in JSO frame.

5 COMET HALLEY

The mean polarization degree of *low resolution* is 4.5 %, while it can reach 10 % to the most and almost 0 to the least. (see Fig.9 *left*) The mean polarization degree of *high resolution* is 6.8 %, while it can reach 15 % to the most and almost 0 to the least. (Fig.9 *right*) Since comets are cruising around the interplanetary space, it's efficient to detect the magnetic field of some particular area by tracing a comet.

6 DISCUSSION

Although we focus on the emission line of Na D1 and D2, there are abundant lines alignable in prominent universe lines. In other words, this method is practical to detect magnetic field of the interplanetary, interstellar and intergalactic space. It also can be used for the magnetic field in QSOs and other objects. As long as the magnitude of the magnetic field is sub-gauss and the collisional rate is not too high.

Atom alignment is sensitive to the orientation of the magnetic field. We can acquire the entire information of the magnetic field with two or more alignable lines.

The resolution of our synthetic observation is limited by the spacecraft's interval of detection. The space resolutions employed in the synthetic observation are Fig.4 *left* 6.3×10^5 km and Fig.8 *left* 1.01×10^4 km. Compared with the image a fine telescope can obtain in interplanetary space, they are too rough. For example the Steward MMT with resolution 0.018 arcsec at the wavelength of $0.5 \mu\text{m}$ (see Strittmatter et al. (1979)), can resolve the interval less than 100 km when take pictures around Jupiter. Hence, the real observation can be quite precise even more than the spacecrafts. In addition, the figure of all the parameters shown above seem much more like broken lines rather than curves also because the big interval between two data points.

Since it's quite easy to translate the polarization information to the magnetic information, we can obtain the instantaneous tomography

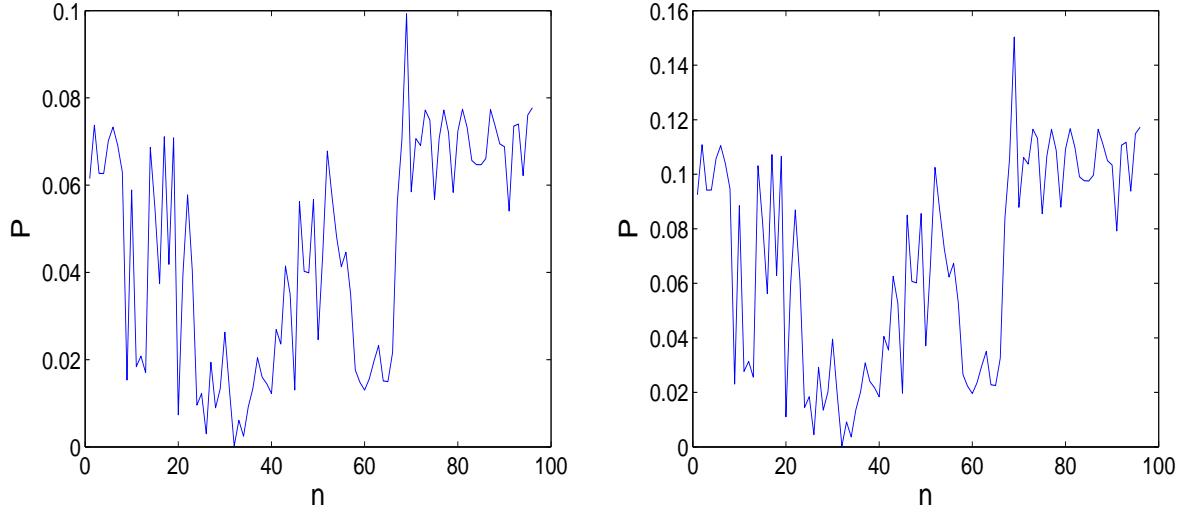


Figure 9. *Left:* the polarization degree of *low resolution*. *Right:* the polarization degree of *high resolution*. n of the x-axis is the sequence number of the data corresponding to Fig.8 left.

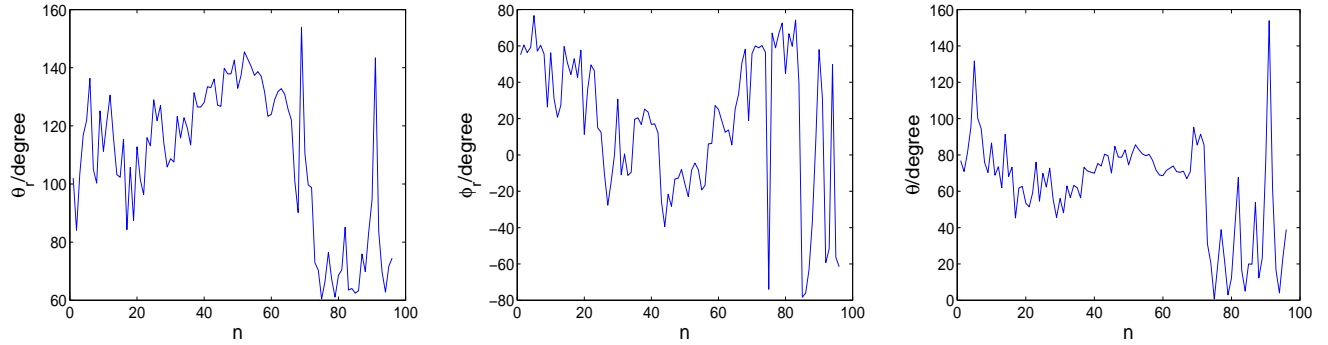


Figure 10. *Left:* θ_r , the angle between incident radiation and magnetic field see Fig.2 left and Fig.3 right. *Middle:* ϕ_r , the azimuth of the incident radiation corresponding to θ_r in the theoretical frame. *Right:* θ , the angle between the observational direction and the magnetic field.

of the magnetic field, which is important to observe the evolution of particular magnetic field directly. Furthermore, it's possible to acquire the 3D topology of the magnetic field.

7 SUMMARY

1. Atoms and ions with fine or hyperfine structure ($J > 1$) can be aligned in their ground state, providing a promising method to detect the weak magnetic fields, especially the orientation, in diffused medium.

2. The polarization degree P and the angle between the magnetic field and the polarization χ are determined by the position angles of pumping source and the observer.

3. The magnetic field magnitude does not apparently limit the polarization degree, insuring the method's validity for weak magnetic field.

4. In general, the polarization degree P varies from 0 to 15 %.

5. The resolution of the spectrometer doesn't limit the accuracy of detecting the orientation of the magnetic field.

6. The resolution of detecting magnetic field with this method is determined by the resolution of the telescope. The accuracy can be even higher than the space probe.

7. Atomic alignment allow us to obtain the instantaneous tomography of the magnetic field.

8 ACKNOWLEDGEMENT

Huirong Yan and Jinyi Shangguan are supported by the "985" program of Peking University.

REFERENCES

- McComas, D.J., et al., Science 326, 959, 2009
Funsten, H.O. et al. 2009, Science, 326, 964
Hawkins, W. B.1955, Phys. Rev. 98, 478
Heerikhuisen, J. et al.2010, ApJ, 708, L126
Kivelson, M.G., Khurana, K.K., Russell, C.T., Walker, R.J., Joy, S.P., Mafi, J.N., GO JUPITER MAG MAGNETOSPHERIC SURVEY V1.0, GO-J-MAG-3-RDR-MAGSPHERIC-SURVEY-V1.0, NASA Planetary Data System, 1997
Schwadron, N.A.,et al. 2009, Science, 326, 966
Ston, E.C. et al. 2005, Science, 309, 2017
Strittmatter, P.A., 1979SAOSR. 385..163S
Varshalovich, D. A. 1968, Astrofizika, 4, 519
Yan, H. & Lazarian, A. 2006, ApJ, 653, 1292
Yan, H. & Lazarian, A. 2007, ApJ, 657, 618
Yan, H. & Lazarian, A. 2008, ApJ, 677, 1401